Tunable damping in the Heusler compound $Co_{2-x}Ir_xMnSi$

Albrecht Köhler, Lukas Wollmann, Daniel Ebke, and Stanislav Chadov
Max Planck Institute for Chemical Physics of Solids, Noethnitzer Str. 40, 01187 Dresden, Germany

Christian Kaiser, Zhitao Diao, Yuankai Zheng, and Qunwen Leng
Western Digital Corporation, 44100 Osgood Road, Fremont, California 94539, USA

Claudia Felser*
Max Planck Institute for Chemical Physics of Solids, Noethnitzer Str. 40, 01187 Dresden, Germany
(Received 8 October 2015; revised manuscript received 7 January 2016; published 9 March 2016)

Here we report on the realization of tuning the intrinsic damping in the half-metallic Heusler compound Co_2MnSi by substituting Co by Ir. The work includes theoretical calculations and experimental measurements on bulk and thin films samples. Control of damping is to remove unwanted magnetization motion and suppress signal echoes through uncontrolled precession of the magnetization for future implementation of this material into, e.g., current perpendicular plane–giant-magnetoresistance sensors. Density functional calculations revealed stable magnetization and increasing damping parameter with Iridium concentration, whereas the half metallicity could be retained. The calculations are consistent with experimental results from bulk and thin film samples of this report and elucidate the linear dependence of the Gilbert damping parameter on the substituent concentration. This report again demonstrates the inherent tunability of Heusler compounds, which constitutes a pivotal feature of this material class.

DOI: 10.1103/PhysRevB.93.094410

I. INTRODUCTION

Tremendous progress has been achieved in the development of spintronics devices such as magnetic random access memory (MRAM), current perpendicular plane–giant-magnetoresistance (CPP-GMR), and spin transfer torque random access memory (STT-RAM) based technologies in the last decade. The Heusler compound Co_2MnSi (CMS) [1,2], is a prominent and well-studied candidate for tunnel-magnetoresistance (TMR) [3–5], CPP-GMR [6,7], and STT-RAM [8] spintronics devices and recently a spin polarization of at least 93% has been reported [9]. It furthermore constitutes a robust half metal (HM) that is unaffected by $B2$ disorder [10]. Tunability of the Gilbert damping parameter α [11,12] in the applied materials is a crucial step towards controlling switching behavior and thus the efficiency of the device. Fast relaxation of the magnetization into equilibrium without *ringing*, i.e., an excessive precession of the magnetization vector [13], is desirable. There have been different approaches, i.e., modifying composition by rare-earth doping [14–16], which, however, leads to increasing film amorphization. There were efforts in changing CMS composition by adding Co in $Co_{2(1+x)}Mn_{1-x}Si_{1-x}$ [17], which leads to a reduction of half metallicity [18,19] and increase of intrinsic damping parameter α by introducing Co antisites [20]. However, it has not been attempted to tune the intrinsic damping while at the same time maintaining HM properties. Here we report on the controlled tuning of intrinsic damping of the HM Heusler compound CMS by means of substituting Co with the isoelectronic element Ir, leading to $Co_{2-x}Ir_xMnSi$ (CIMS) up to $x_{Ir} = 0.5$ (bulk) and 0.54 (thin films). We combined theoretical calculations, bulk ingot preparation, and sputtered thin films of this novel quaternary Heusler compound. We found damping to be linearly increasing with substituent concentration whereas maintaining the saturation magnetization (M_{sat}) in bulk and half metallicity in theory.

II. CRYSTAL STRUCTURE

Co_2MnSi crystallizes in the $L2_1$ structure, i.e., cubic space group 225 ($Fm\bar{3}m$), where Co occupies Wyckoff position 8c (1/4, 1/4, 1/4) and Mn and Si are located at 4b (1/2, 1/2, 1/2) and 4a (0, 0, 0), respectively [Fig. 1(a)]. The substitution of Co by Ir is accounted for in representing position 8c by mixed occupation retaining the symmetry of SG 225 [Fig. 1(b)].

III. COMPUTATIONAL DETAILS

The numerical work was done using the fully relativistic implementation of density functional theory (DFT) in the framework of the KKR Green's function formalism as implemented in the Munich SPR-KKR package [21]. To conveniently describe the random Co-Ir substitution, the coherent potential approximation (CPA) [22,23] has been utilized for an efficient treatment of the chemical disorder. The self-consistent-field (SCF) calculations were converged on a $42 \times 42 \times 42$ k-point grid leading to 9743 k-points in the irreducible wedge of the Brillouin zone. The angular momentum expansion of the wave functions was truncated for $l_{max} = 3$ (corresponding to f symmetry), whereas the energy integration was carried out on a path of 48 energy points in the complex energy plane. The parametrization of the generalized gradient approximation (GGA) to exchange-correlation functional of Perdew, Burke, and Enzerhof [24] was chosen. The temperature and x_{Ir} dependency of the Gilbert-damping parameter α was evaluated from first-principles on the basis of the converged SCF calculations making full use of the underlying electronic

*Claudia.Felser@cpfs.mpg.de

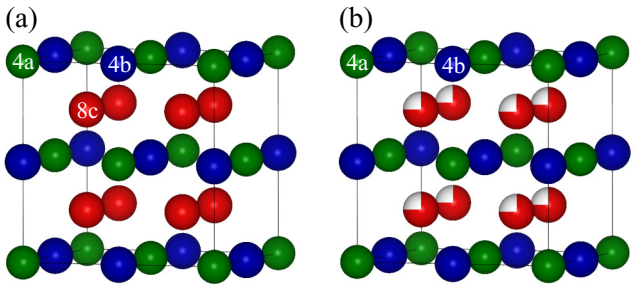

FIG. 1. The crystal structures of (a) Co_2MnSi and (b) $Co_{2-x}Ir_xMnSi$. A partial substitution of Co by Ir is shown. In contrast to a supercell approach, the substitution is realized through a mixed occupation of atomics sites.

structure. The damping parameter is computed through a parameter-free Kubo-Greenwood-like expression provided by Ebert *et al.* [21,25,26] that has been shown to be equivalent to Kambersky's torque correlation model (TCM) and exploiting the reformulation of the TCM in terms of scattering theory by Brataas *et al.* [27]. Compared to previously conducted studies within the TCM, the formulation in terms of scattering theory and DFT allows us to conveniently calculate α without the unpleasant necessity of a phenomenological parameter, such as the scattering life time τ. On the basis of the implemented CPA formalism for the treatment of disordered systems, α could be determined as function of doping concentration. The experimental lattice parameters of the here synthesized bulk samples of the corresponding Ir concentrations served as input for the electronic structure calculations. Existing data points were linearly interpolated for other concentrations for which information from experiments was not available. Additionally, thermal fluctuations of the lattice and their influence on α have been accounted for via an alloy-analogy-model that accounts for finite-temperature effects via quasistatic random displacements of the atomic sites [26]. For the calculation of these a fine k-mesh with $179 \times 179 \times 179$ points was set up. For each compound $Co_{2-x}Mn_xSi$ the temperature dependence $\alpha(T)$ was scanned in a range $0 \leqslant T \leqslant 400$ within 30 steps. The calculations were done for a set of 16 different Ir concentrations $0 \leqslant x_{\mathrm{Ir}} \leqslant 0.75$ to obtain a dense sampling of the dependency of α.

IV. EXPERIMENTAL DETAILS

Polycrystalline bulk ingots were prepared via arc melting and analyzed with x-ray diffraction (XRD; Cu-K_α), superconducting quantum interference device-vibration sample magnetometry (SQUID-VSM), differential scanning calorimetry (DSC), and scanning electronic microscopy (SEM) for phase analysis/inclusions. Their degree of $B2$ and $L2_1$ ordering is evaluated by order parameter $A_{\mathrm{B2/L2_1}}$:

$$A_{\mathrm{B2}} = \frac{I(002)/I(004)}{I_0(002)/I_0(004)}, \quad A_{\mathrm{L2_1}} = \frac{I(111)/I(022)}{I_0(111)/I_0(022)}, \quad (1)$$

where I and I_0 are the corresponding experimental and theoretical integrated XRD peak intensities, respectively.

Polycrystalline CIMS thin films were deposited onto thermally oxidized Si wafers via a commercial Anelva Sputter System, complying with the industrial requirements for growing films on amorphous substrates. Two 4 in. targets with the composition Co_2MnSi and Ir_2MnSi were DC cosputtered onto 8 in. thermally oxidized Si wafers. The stacking is *subs.*/30Ta/20Ru/180CMS/20Ru (numbers in Å), where the seed layers create a strong (011) texture. The films were crystallized *in situ* via rapid transfer annealing (RTA) without breaking the vacuum at temperature $T_a = 500\,^{\circ}\mathrm{C}$ for 600 seconds before they were finally capped with a protective Ru film. Thin film composition was measured by x-ray fluorescence (XRF), which was calibrated via Rutherford backscattering (RBS). Crystal structure was investigated via x-ray diffraction (XRD) and surface morphology was controlled via atomic force microscopy (AFM). A B-H looper (BHL) was used to obtain magnetization loops and M_{sat}. The damping was measured via ferromagnetic resonance (FMR) lock-in detection method with Helmholtz-modulation coils [28], a coplanar waveguide [29], and a microwave signal generator. The data points were collected for in- and out-of-plane geometry (IP/OP or $\parallel/\perp$) with external field H saturating the sample, so that $d\mathrm{M}/dH \cong 0$ ($H > 3\mathrm{kOe} + \mathcal{N}4\pi M_{\mathrm{eff}}$, with the demagnetization tensor $\mathcal{N}$).

The FMR output is the derivative of the absorbed power, i.e., the imaginary part of the magnetic susceptibility $d\chi''/dH$, and is fitted to an asymmetric Lorentzian, which takes coupling between the sample and the waveguide into account. The fitted resonance frequency position H_{res} is plotted vs. resonance frequency f via the modified Kittel equation omitting uniaxial and magnetocrystalline anisotropy due to random in-plane crystal orientation to obtain the effective magnetization (M_{eff}) [30,31]. For IP we have

$$f = \frac{\gamma}{2\pi}\sqrt{H_0(H_0 + 4\pi M_{\mathrm{eff}})}, \quad (2)$$

where $4\pi M_{\mathrm{eff}} = 4\pi M_{\mathrm{sat}} - 2K_{\mathrm{U}}^{\perp}/M_{\mathrm{sat}}$ and $K_{\mathrm{U}}^{\perp}$ is the perpendicular uniaxial anisotropy constant [32]. Additional to a possible perpendicular magnetic anisotropic contribution, a difference between M_{sat} and M_{eff} can arise from the magnetic-volume-sensitive BHL measurement in contrast to the magnetic-volume-independent FMR technique. If there is nonmagnetic volume present in the film, i.e., a magnetically dead layer with thickness t_{dl} at an interface, then generally $M_{\mathrm{eff}} > M_{\mathrm{sat}}$. By measuring t_{dl} one can introduce the corrected saturation magnetization $M_{\mathrm{sat}}^{*} = M_{\mathrm{sat}} \times t/(t - t_{\mathrm{dl}})$, where t is the film thickness.

For the OP FMR response we have

$$f = \frac{\gamma}{2\pi}(H_0 - 4\pi M_{\mathrm{eff}}), \quad (3)$$

where we omitted $K_1^{\perp}$.

The IP FMR linewidth can be expressed as

$$\Delta H_{\parallel} = \frac{4\pi\alpha}{\sqrt{3}\gamma} f + \Delta H_{2\mathrm{M}}(f) + \Delta H_{0,\parallel}, \quad (4)$$

where the first part denotes the intrinsic Gilbert damping (with the intrinsic damping parameter α) due to magnon-electron scattering and $\Delta H_{2\mathrm{M}}(f)$ the extrinsic broadening connected to two-magnon scattering (2M). The latter arises from weak interactions between the spin-wave modes that effectively allow energy dissipation of the uniform precession

into other modes [33]. Additionally, imperfections generate the frequency-independent extrinsic contribution ΔH_0, due to microstructural differences such as local anisotropies or magnetostriction. Here, random inhomogeneities spread the linewidth by the superposition of multiple local FMR absorption profiles [34,35]. Following [36] the 2M contribution can be expressed as

$$\Delta H_{2M}(f) = \Gamma \sin^{-1} \sqrt{\frac{\sqrt{f^2 + (f_0/2)^2} - (f_0/2)}{\sqrt{f^2 + (f_0/2)^2} + (f_0/2)}}, \quad (5)$$

where Γ is the strength of the two-magnon scattering and $f_0 = 2\gamma M_{\text{eff}}$. This line-broadening type reveals itself when $\Delta H(f)$ data shows a curvature.

Quenching of the 2M contributions in the OP FMR configuration [35] leads to the expression for the OP line broadening

$$\Delta H_{\perp} = \frac{4\pi\alpha}{\sqrt{3}\gamma} f + \Delta H_{0,\perp}. \quad (6)$$

We will use the superscripted symbols $\parallel$ and $\perp$ for M_{eff} and α to clarify the used measurement configuration (in theory these quantities are the same).

We would like to point out that the choice of seed/material was crucial for a systematic investigation. FMR measurements on, e.g., Cr-buffered samples (not shown here) show a strong variation in damping with annealing temperature. Reported increasing diffusion of Cr into the Heusler for $T_a > 450\,^{\circ}$C [6,37] and additional interfacial anisotropy [38] has profound impact onto the magnetization dynamics and thus impedes a systematical investigation of $\alpha(x_{\text{Ir}})$ for Cr-buffered C(I)MS films.

V. RESULTS

A. Bulk

Table I shows M_{sat}, T_{C} and lattice constants for the bulk samples. There are slight variations in M_{sat}, which are not attributed to x_{Ir} but most likely originate from arc melting parameter adjustments due to increasing Ir content. T_{C} decreases about 100 K and the lattice parameter increases by 1% when going from Co_2MnSi towards $Co_{1.75}Ir_{0.25}MnSi$. For $x_{\text{Ir}} > 0.25$, a secondary Ir-rich phase develops, which cannot be cured by subsequent melting and annealing for several days (Fig. 2). XRD $2\theta/\omega$ scans, Fig. 3, reveal this phase separation with the appearance of broad peak shoulders and newly emerging peaks.

TABLE I. Magnetization and lattice constant a of the bulk samples.

x_{Ir}	a (Å)	M (μ_{B}/f.u.) @1.8 K/298 K	T_{C} (K)
0.00	5.660	5.0/5.0	1008
0.05	5.672	4.9/4.7	987
0.10	5.681	4.7/4.6	983
0.20	5.704	5.2/5.0	943
0.25	5.711	5.0/4.7	923
0.50	5.721	n.a.	n.a.

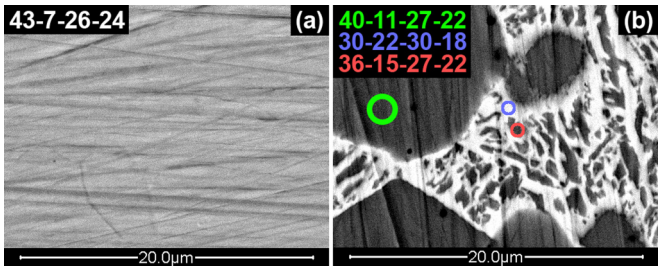

FIG. 2. SEM phase contrast images, numbers are at% composition Co-Ir-Mn-Si: (a) $x_{\text{Ir}} = 0.25$, single phase only; (b) $x_{\text{Ir}} = 0.5$, phase separation (green and blue) and intermediate phase (red).

B. Electronic structure calculations

The calculations resulted in ferromagnetic ground states for all systems in this study, thus obtaining the measured saturation magnetization (Table I) confirming our calculations. Indeed, the situation for increased x_{Ir} did not change the situation dramatically referring to the static magnetic properties as compared to CMS. Due to the introduction of Ir the total spin magnetic moment varies in a range of 4.952 μ_B and 4.924 μ_B, which is more or less negligible. Thus, the local moments of Mn and Co are enhanced, compensating the loss of Co (as seen in Table II). Figure 4 visualizes the effect of Ir substitution in terms of the electronic structure. Band structures of the CMS phase and the heavily substituted phase $Co_{1.25}Ir_{0.75}MnSi$ are visualized along the direction L–Γ–X. Due to the substitution of Co, the shown bands are broadened, whereas the majority bands below the Fermi energy (ε_F) are more strongly broadened than the minority states. From the projected DOS, the contributions of Ir states can be seen as emergence of spectral weight with Ir character.

Despite the broadening of the minority bands at ε_F, the substitution does not destroy the half-metallic properties, as the semiconducting gap in the minority spin channel is retained, having a width of about $\Delta E_{\text{gap}} \approx 0.5$eV.

Gilbert Damping

The calculations of α lead to the results depicted in Fig. 5 and 6. Figure 5 visualizes the dependency of the α on temperature variations in detail. The change of α with increasing temperature is remarkably small. The only

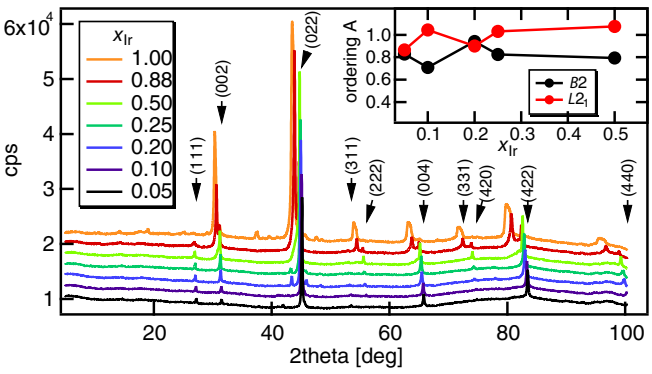

FIG. 3. XRD $2\theta/\omega$ scans for polycrystalline bulk samples for increasing substitution of Co by Ir.

TABLE II. The local moments (μ_B) and the magnetization (μ_B/f.u.) are shown in relation to x_{Ir}. Their deviation from the parent phase is small for the complete substitutional range.

x_{Ir}	m_{Co}	m_{Ir}	m_{Mn}	m_{Si}	m_{spin}	m_{orb}	m_{tot}
0.00	0.960		3.141	−0.110	4.952	0.072	5.024
0.05	0.970	0.216	3.156	−0.109	4.949	0.072	5.021
0.10	0.983	0.218	3.164	−0.106	4.947	0.072	5.019
0.20	1.005	0.219	3.193	−0.103	4.943	0.072	5.014
0.30	1.035	0.225	3.209	−0.098	4.939	0.071	5.010
0.40	1.069	0.234	3.222	−0.091	4.936	0.070	5.006
0.50	1.105	0.245	3.236	−0.084	4.933	0.070	5.003
0.60	1.143	0.256	3.252	−0.076	4.929	0.069	4.999
0.70	1.182	0.269	3.269	−0.068	4.926	0.069	4.995
0.75	1.202	0.275	3.278	−0.064	4.924	0.069	4.993

exception seen is the pure compound CMS, for which $\alpha(T)$ steeply increases in the low-temperature limit, which is a well-known effect for pure compounds as the scattering lifetime τ is increasing in the low-temperature regime [39]. In this case, the low-temperature Gilbert damping is related to intraband contributions while the interband spin-flip scattering is responsible for the high-temperature dissipation. As the first effect is spin conserving it can be pronounced even for half-metallic systems, as in the present case. However, the contribution of spin-flip scattering at high temperatures is rather small due to the energy gap at ε_F in the minority spin channel.

As has been shown earlier [25], slight imperfections in the crystalline order of the studied materials suppresses the steep increase at low T, thus leading to a finite value of α. In the present work, it is seen that substitution of Co by at least 5% Ir completely quenches this effect. Small amounts of Ir substituent lead to a strong decrease of α at low temperatures as well as to its weak dependence on T in general.

CMS is an ideal model system to unravel the different proportionalities of α due to its peculiar electronic structure, that exhibits only two majority bands at ε_F. From the band-structure calculations we conclude, that interband (spin-flip)

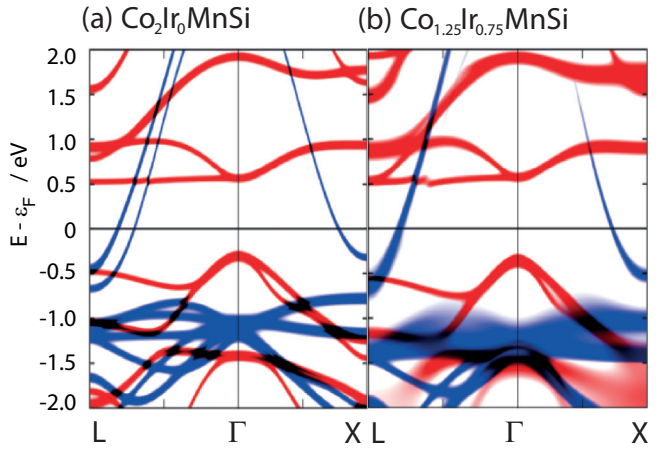

FIG. 4. The band structures of (a) Co_2MnSi and (b) $Co_{1.25}Ir_{0.75}MnSi$ are shown. Despite the substitution the half-metallic character is maintained: blue: majority states; red: minority states.

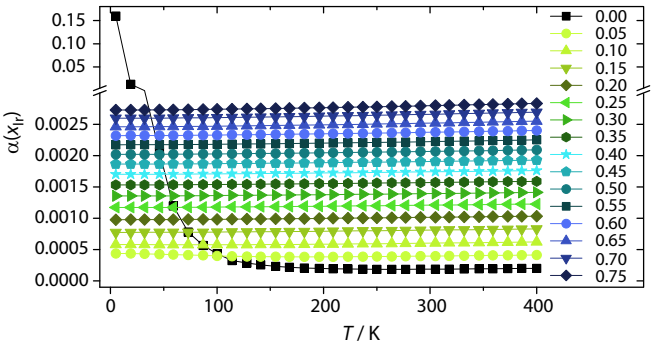

FIG. 5. The temperature dependence of the calculated damping parameter α is shown for a set of substitution concentrations x_{Ir}.

contributions are strongly suppressed due to the peculiar electronic properties of half-metallic $Co_{2-x}Ir_xMnSi$.

Besides the temperature dependence, α has been studied according to the substitution of Co through Ir. We found a linear relationship between x_{Ir} and the calculated values for α at a exemplary temperature of $T = 277$ K. The change of α with temperature is considered to be negligible from the earlier observation, and thus the linear relation between α and x_{Ir} is valid over the whole temperature range. Replacement of Co by Ir was shown to lead to minor modifications in terms of the magnetic moments only (Table II), nevertheless the effect on dynamical properties as α is considerable. The near room-temperature ($T = 277$ K) values for α were linearly tuned by

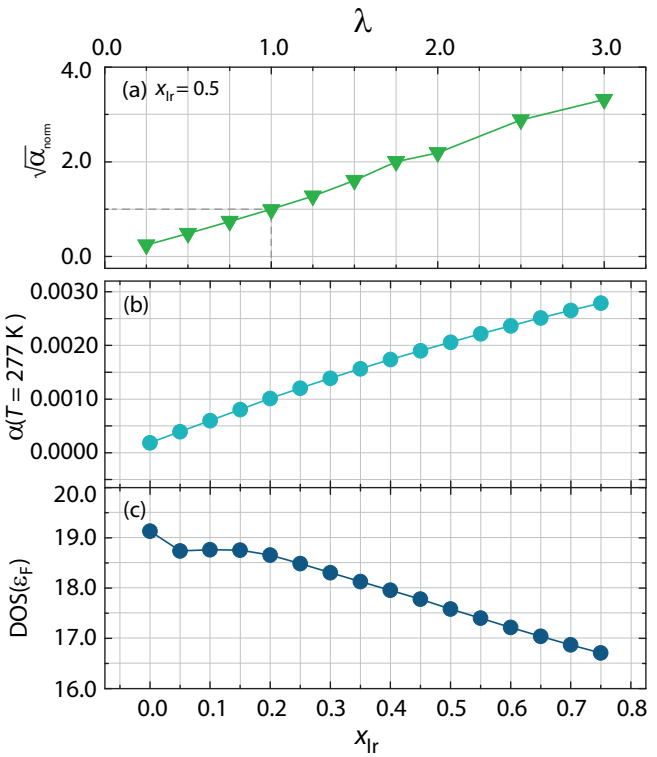

FIG. 6. (a) Dependence of $\alpha(x_{Ir} = 0.5)$ on the spin-orbit coupling parameter. (b) Dependence of $\alpha(x_{Ir}, T = 277\ \text{K})$ on the Ir concentration. (c) Variation of the DOS at ε_F with increasing Ir content, x_{Ir}.

substitution over one order of magnitude ($1.87 \times 10^{-4} \leqslant \alpha \leqslant 2.79 \times 10^{-3}$).

As a linear dependence of $\alpha(x_{\mathrm{Ir}})$ is obtained from our calculations, α has been calculated as function of the spin-orbit coupling strength that is represented in terms of the spin-orbit coupling (SOC) parameter λ_{so} for one exemplary system, $Co_{1.5}Ir_{0.5}MnSi$. Here λ_{so} was artificially scaled in the range of $0.25 \leqslant \lambda_{\mathrm{so}} \leqslant 3$. From these calculations, it is seen [Fig. 6(a)] that α shows a quadratic dependence on λ_{so}. Similar observations have been reported from experiments on $FePd_{1-x}Pt_x$ thin films [40] and theoretically for bulk Permalloy +15% Os [25] before. Gilbert damping is phenomenologically depending on the shape of the DOS. It is thus expected to find smaller values, of α in consequence of small spectral weight. In the present work, the DOS(ε_F,x) is linearly reduced for increasing Ir content. We thus expect this effect to counteract on the increasing SOC that is distinctly different from the behavior found in the $FePd_{1-x}Pt_x$ samples.

C. Thin films

Magnetization loops are shown in Figs. 7(a)–7(c).

Thickness-dependent magnetization measurements of CMS, see Fig. 8(a), gives a thickness for the magnetic dead layer of $t_{\mathrm{dl}} = 8$ Å, which is used to correct $M_{\mathrm{sat}} \rightarrow M^*_{\mathrm{sat}}$, as described in Sec. IV. We assume t_{dl} to be constant throughout the range of Ir content. Figure 8(b) shows the intrinsic damping of CMS for different thicknesses. We find a similar behavior as

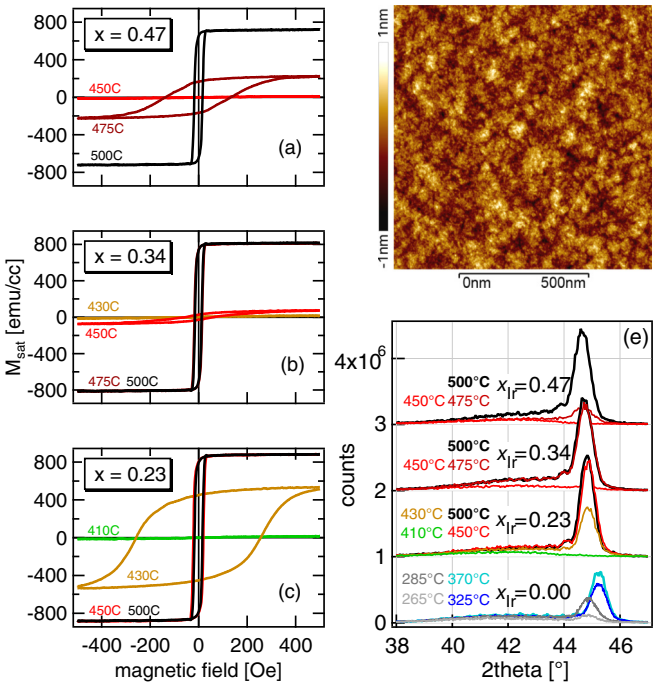

FIG. 7. Magnetic properties, AFM image and and XRD scans of the prepared films: (a)–(c) Magnetization loops (BHL) for three compositions with increasing Ir content, different RTA anneal steps. (d) AFM image of sample with $x_{\mathrm{Ir}} = 0.23$. (e) $2\theta/\omega$ XRD scans of the same samples as in (a)–(c). The (0002) peak of the 20 Å Ru seed is broad and around 42.2°, adjacent to the (002) Heusler peak (substrate peak not shown).

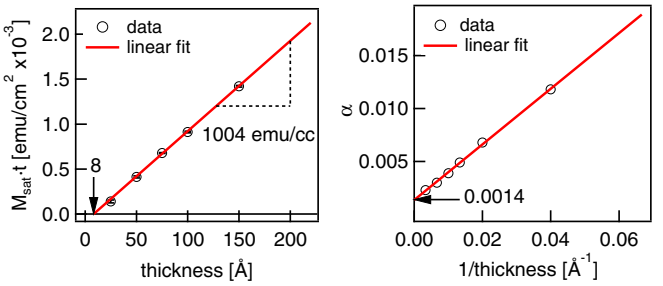

FIG. 8. Thickness-dependent measurements of *subs.*/30Ta/20Ru/xCMS/20Ru for (a) the magnetization reveal a 8 Å thick magnetically dead layer for CMS. (b) α scales inversely with the film thickness.

reported in Ref. [52], where the intrinsic damping parameter is found to be dependent on the film thickness.

XRD $2\theta/\omega$ scans in Fig. 7(e) show only the substrate and (022) Heusler peak. There is a saturating jump for the (022) reflex after annealing at a specific minimal temperature $T_{\mathrm{a}}^0(x_{\mathrm{Ir}})$, which increases with x_{Ir}. Since there is no apparent XRD-peak degeneration with increasing x_{Ir}, amorphization can be excluded. In fact, the peak intensity is rising with x_{Ir} due to an increasing atomic form factor which proves the integration of Ir atoms into the Heusler lattice. The films are 2−3 % strained in the c direction as compared to the bulk lattice parameters due to the smaller in-plane atomic distance in the (0002) Ru plane. Crystallite size obtained via the Scherrer formula [41] is increasing with temperature and equals film thickness at $T_{\mathrm{a}}^0(x_{\mathrm{Ir}})$. (022) rocking curves (not shown here) gave FWHM $\simeq 4.5°$, negligibly depending on annealing temperature, which corresponds to a minimum lateral coherent scattering crystallite size of $\simeq$25 Å, accompanied by broadening due to mosaicity. This indicates distinct columnar growth that is induced by the Ta/Ru seed layer. The typical surface roughness is $R_{\mathrm{q}} = 2$ Å, even after annealing.

M_{sat} of CMS is linked to the crystal structure of CMS, that develops generally as $amorph. \mapsto A2 \mapsto B2 \mapsto L2_1$ with increasing temperature T_{a} [42]. Since randomly distributed atoms ($A2$ disorder) lead to poor M_{sat} [43] and the fact that in our case M_{sat} is not changing when $T_{\mathrm{a}} > T_{\mathrm{a}}^0$, we can associate T_{a}^0 with formation of a $B2$ phase, which leads to a high magnetization curve with low coercivity, see Figs. 7(a)–7(c). We further know that $T_{\mathrm{a}} > T_{\mathrm{a}}^0$ eventually leads to $L2_1$ order [44], which has to be investigated via direct structural measurement techniques and will not be quantified within the scope of this report. However, we found that for $T_{\mathrm{a}} > T_{\mathrm{a}}^0$, all measured film properties for any x_{Ir} are absolutely independent of T_{a}. This hints towards successful $B2/L2_1$ mixed crystallization in our case, since the magnetic properties, e.g., damping, are sensitively dependent on the structural ordering [37].

Figure 9 shows the IP FMR response and fitted data (OP FMR data not shown here). The resonance positions $f(H_{\mathrm{res}})$ were fitted via Eq. (2). We would like to point out that fitting IP FMR $f(H_{\mathrm{res}})$ is very sensitive to the chosen range, which can lead to a comparably large uncertainty in $M_{\mathrm{eff}}^{\parallel}$ [31]. We accounted for that by fitting within different ranges and including an error for $M_{\mathrm{eff}}^{\parallel}$. We further find that the fit following

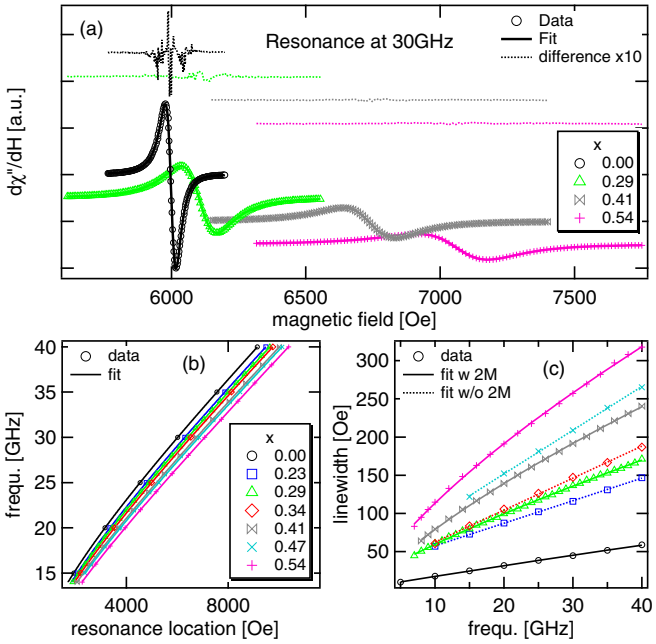

FIG. 9. (a) IP FMR response, asymmetric Lorentzian fit and difference for selected Ir concentrations. The curves are shown with an offset for better visibility. (b) (zoomed in) Using results from (a) and fitting it using the solution to the LLG equation Eq. (2). (c) Fit for α and Γ with Eq. (4). For the samples with $x_{\mathrm{Ir}} = 0.23$, 0.34, and 0.47 a linear fit without the 2M term was performed.

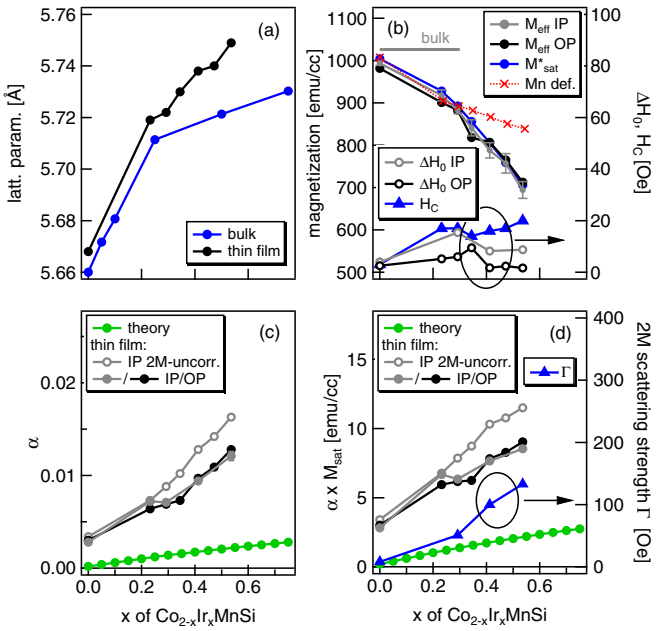

FIG. 10. (a) Film/bulk lattice parameter obtained via XRD. (b) M^*_{sat} and M_{eff} (IP and OP FMR configuration), H_c and extrinsic contributions ΔH_0 (IP only). The red curve is the expected trend for a linearly increasing Mn depletion of 5 at% within this range. (c) Intrinsic damping $\alpha^{\parallel/\perp}(x_{\mathrm{Ir}})$. (d) Product of $\alpha^{\parallel/\perp}$ with associated M_{eff}.

Eq. (3) for the OP case is less sensitive to the chosen range, leading to a smaller error in $M^{\perp}_{\mathrm{eff}}$. α was evaluated following Eqs. (4) and (6), depending on the FMR configuration. For the IP case $\Delta H_{2\mathrm{M}}(f)$ can be difficult to extract for $\Delta H(f)$ data with small curvature, since the fit handles all line-broadening contributions independently. We therefore present two types of fits for the IP linewidth data: one that includes the expression for $\Delta H_{2\mathrm{M}}(f)$, thus giving $\alpha_{\parallel}$, and one that omits it, where in the latter case the resulting 2M-uncorrected-$\alpha^{\parallel}$ is effectively enhanced, see Figs. 10(c) and 10(d). We find that the inclusion of the $\Delta H_{2\mathrm{M}}(f)$ term into the fit leads to a very good agreement of $\alpha^{\parallel}$ with $\alpha^{\perp}$, but only if there are data points in a wide enough frequency range [36], thus validating this approach even for less apparent curvatures in $\Delta H(f)$.

Lattice constant a, M_{sat}, H_c $M^{\parallel/\perp}_{\mathrm{eff}}$, ΔH_0, $\alpha^{\parallel/\perp}$, $\alpha^{\parallel/\perp} \times M_{\mathrm{sat}}$, and Γ are shown in Figs. 10(a)–10(c). There was a slight compositional difference of the resulting films from the two targets, which inevitably induced an increasing Mn deficiency up to 5 at% (20 at% instead of 25 at% in the compound) for $x_{\mathrm{Ir}} = 0.54$. This monotonically reduces M_{sat} [5] since the Mn positions carry the main contributing magnetic moment. However, the reduction of M_{sat} with x_{Ir} is about twice as strong as the estimation based on a simple removal of Mn from the octahedral positions predicts, as included in Fig. 10(b). We therefore suspect increasing antisite disorder that additionally reduces the magnetic moments of the neighboring atoms. Since $\alpha = G/(\gamma M_{\mathrm{sat}})$ [45], with G being the Gilbert constant, we phenomenologically accounted for the Mn-depletion-related loss of magnetization by evaluating $\alpha \times M_{\mathrm{sat}}$, that trends linearly with x_{Ir}. The proportionality of the experimental data for $\alpha M_{\mathrm{sat}}(x_{\mathrm{Ir}})$ is less drastic as $\alpha(x_{\mathrm{Ir}})$ and more comparable to the theoretical slope, but still about a factor 2 larger.

Table III summarizes thin film data obtained by XRD, BHL, and FMR measurements. We note that $g^{\perp} \simeq g^{\parallel} \equiv g$ (difference in $g < 2\%$).

VI. DISCUSSION

The calculated values for α are significantly smaller than previously reported first-principles calculations ($\alpha = 6 \times 10^{-5}$) [46] where a phenomenological scattering parameter on basis of the residual resistivity was used. However, we point out that in this work the CMS sample ($T_a = 370\,^{\circ}\mathrm{C}$) exhibits $\alpha(x_{\mathrm{Ir}}) = 0.003$. This is one magnitude smaller than for previously reported CMS polycrystalline samples ($\alpha = 0.025$) [47]

TABLE III. Lattice constant a, M_{sat}, damping parameter $\alpha_{\parallel}$ and $\alpha_{\perp}$ for IP and OP FMR configuration (respectively), two-magnon scattering strength Γ obtained from the IP data and the averaged g factor of the thin film samples at ambient temperature. The values for $\alpha^{\parallel}$ printed in *italic* are the results from a linear regression where the 2M term in Eq. (2) was omitted, which clearly leads to an overestimation of the intrinsic damping by comparison with $\alpha^{\perp}$.

x_{Ir}	a (Å)	M (μ_{B}/f.u.)	$\alpha^{\parallel}$	$\alpha^{\perp}$	Γ (Oe)	g
0.00	5.668	4.9	0.0031	0.0030	8	2.034
0.23	5.719	4.7	*0.0073*	0.0064	n.a.	2.027
0.29	5.722	4.5	0.0071	0.0069	51	2.025
0.34	5.730	4.3	*0.0128*	0.0073	n.a.	2.033
0.41	5.738	4.1	0.0095	0.0097	100	2.025
0.47	5.740	3.9	*0.0142*	0.0109	n.a.	2.032
0.54	5.749	3.6	0.0121	0.0128	133	2.030

and even smaller than obtained for high-quality epitaxial samples with $B2$ [37] or $L2_1$ order where ($\alpha = 0.0054$) [48], in fact it is the lowest reported α to date for a CMS film with a thickness below 20 nm. This hints towards a high spin polarization for this sample [49], which will be further investigated. The high value for $M_{\mathrm{sat}} = 1004\mathrm{emu/cc}$ supports this argument. In any case, $B2$ disorder maintains HM [10], which eases up the requirements from an applicational perspective.

Process-related Mn deficiency leads to a reduction of M_{sat} with increasing x_{Ir} and results in an additional contribution to α due to Co antisites, similarly to the Co off-stoichiometric in CMS presented by Yang *et al.* [20]. For $x_{\mathrm{Ir}} = 0$ we observe that $M_{\mathrm{eff}} < M_{\mathrm{sat}}$ indicating a positive $K_{\mathrm{U}}^{\perp}$, which decreases with the addition of Ir, Fig. 7. The dependence of $\alpha(x_{\mathrm{Ir}})$ altogether follows the approximately linear theoretical predictions, but shows an offset and a slightly more drastic proportionality. This is observed in other transition metal systems calculated with the formalism used here as well [25]. We further point out that generally α is thickness dependent [52], see Fig. 8, and one can phenomenologically write $\alpha_{\mathrm{eff}} = \alpha_0 + b/t$ to obtain the bulk intrinsic damping parameter α_0, with a constant b and film thickness t. In this report we did not perform thickness-dependent FMR measurements for CIMS and one has to bear in mind that this thickness dependence can account for the offset of experiment and theory in Fig. 10(d).

A larger homogeneous, intrinsic Gilbert damping is generally connected to increased spin-orbit coupling that results in transitioning from spin waves to single particle states [49]. It is also reported of enhanced intrinsic damping by decreasing the film thickness due to increasing spin-orbit interactions [50]. General modified electronic structure of the thin film in combination with impurity and interface scattering can enhance the Gilbert damping [51]. Other mechanisms that may account for linewidth broadening that is linearly proportional to the frequency are spin pumping [52] or spin-memory loss at the Ru interface [53], which can effectively raise the value of α above bulk. Thus, further investigation, i.e., thickness-dependent measurements for elucidation of interface effects and low-temperature FMR to examine the relaxation at impurities, have to performed to separate the specific line-broadening mechanisms that show a linear proportionality with frequency. Since the thicknesses of the samples are the same, we hypothesize that the interface effects have a negligible x_{Ir} dependence and contribute mostly to the offset of the theoretical to experimental data, see Fig. 10. On the other hand the difference in the slopes (factor 2) is most likely attributed to increasing disorder (impurities).

VII. CONCLUSION

We performed first-principles calculations and prepared bulk and thin films of the novel quaternary Heusler compound $Co_{2-x}Ir_xMnSi$ for different values of x_{Ir} in order to increase the intrinsic damping parameter α of the parent compound Co_2MnSi. We found a theoretical stability of the magnetization with increasing Ir content, which has been confirmed by bulk samples up to a critical Ir concentration. (011)-textured thin film samples confirm a linear increase of the intrinsic damping with Ir(at%), but with larger proportionality as theoretically predicted. We found increasing two-magnon scattering contribution for higher Ir concentration and demonstrated that for a polycrystalline magnetic thin film with random in-plane order it is possible to quantify the two-magnon scattering strength with a simple in-plane FMR measurement. Frequency-independent extrinsic damping is slightly increased but can be cured with appropriate annealing temperature. The successful modification of damping in Heusler compounds while maintaining crucial properties such as structure, magnetization, and HM demonstrates yet again their fascinating tunability that underlines the merit of this material class for spintronic applications.

ACKNOWLEDGMENTS

The authors would like thank S. Hausdorf and S. Mankovsky for fruitful discussions and technical support. Financial support from the Deutsche Forschungsgemeinschaft (DFG; Projects P 1.2-A and P 4.8-A of research unit FOR 1464 "ASPIMATT") and the European Research Council Advanced Grant (ERC-AG; No. 291472 "IDEA Heusler!") is gratefully acknowledged.

The authors A.K. and L.W. equally contributed to this work.

[1] I. Galanakis, P. H. Dederichs, and N. Papanikolaou, Phys. Rev. B **66**, 174429 (2002).
[2] S. Picozzi, A. Continenza, and A. J. Freeman, Phys. Rev. B **66**, 094421 (2002).
[3] Y. Sakuraba, J. Nakata, M. Oogane, H. Kubota, Y. Ando, A. Sakuma, and T. Miyazaki, Jpn. J. Appl. Phys. **44**, L1100 (2005).
[4] H. Liu, Y. Honda, T. Taira, K. Matsuda, M. Arita, T. Uemura, and M. Yamamoto, Appl. Phys. Lett. **101**, 132418 (2012).
[5] G.-f. Li, Y. Honda, H.-x. Liu, K.-i. Matsuda, M. Arita, T. Uemura, M. Yamamoto, Y. Miura, M. Shirai, T. Saito, F. Shi, and P. M. Voyles, Phys. Rev. B **89**, 014428 (2014).
[6] T. Iwase, Y. Sakuraba, S. Bosu, K. Saito, S. Mitani, and K. Takanashi, Appl. Phys. Express **2**, 063003 (2009).
[7] Y. Sakuraba, K. Izumi, T. Iwase, S. Bosu, K. Saito, K. Takanashi, Y. Miura, K. Futatsukawa, K. Abe, and M. Shirai, Phys. Rev. B **82**, 094444 (2010).
[8] L. Tang and Z. Yang, J. Appl. Phys. **114**, 193703 (2013).
[9] M. Jourdan, J. Minár, J. Braun, A. Kronenberg, S. Chadov, B. Balke, A. Gloskovskii, M. Kolbe, H. J. Elmers, G. Schönhense, H. Ebert, C. Felser, and M. Kläui, Nature Commun. **5**, 3974 (2014).
[10] S. Picozzi, A. Continenza, and A. J. Freeman, Phys. Rev. B **69**, 094423 (2004).
[11] T. L. Gilbert, Phys. Rev. **100**, 1243 (1955) [Abstract only; full report, Armor Research Foundation Project No. A059, Supplementary Report, May 1, 1956] (unpublished).].
[12] T. L. Gilbert, IEEE Trans. Magn. **40**, 3443 (2004).
[13] R. H. Koch, J. G. Deak, D. W. Abraham, P. L. Trouilloud, R. A. Altman, Y. Lu, W. J. Gallagher, R. E. Scheuerlein, K. P. Roche, and S. S. P. Parkin, Phys. Rev. Lett. **81**, 4512 (1998).
[14] W. Bailey, P. Kabos, F. Mancoff, and S. E. Russek, IEEE Trans. Magn. **37**, 1749 (2001).

[15] S. G. Reidy, L. Cheng, and W. E. Bailey, Appl. Phys. Lett. **82**, 1254 (2003).
[16] S. Ingvarsson, G. Xiao, S. S. P. Parkin, and R. H. Koch, Appl. Phys. Lett. **85**, 4995 (2004).
[17] Y. Sakuraba, N. Hirose, M. Oogane, T. Nakamura, Y. Ando, and K. Takanashi, Appl. Phys. Lett. **96**, 092511 (2010).
[18] R. A. de Groot, F. M. Mueller, P. G. van Engen, and K. H. J. Buschow, Phys. Rev. Lett. **50**, 2024 (1983).
[19] J. Kübler, A. R. Williams, and C. B. Sommers, Phys. Rev. B **28**, 1745 (1983).
[20] F. Yang, X. Kong, and X. Chen, J. Phys. D: Appl. Phys. **46**, 195001 (2013).
[21] H. Ebert, S. Mankovsky, D. Ködderitzsch, and P. J. Kelly, Phys. Rev. Lett. **107**, 066603 (2011).
[22] P. Soven, Phys. Rev. B **2**, 4715 (1970).
[23] D. W. Taylor, Phys. Rev. **156**, 1017 (1967).
[24] J. P. Perdew, K. Burke, and M. Ernzerhof, Phys. Rev. Lett. **77**, 3865 (1996).
[25] S. Mankovsky, D. Ködderitzsch, G. Woltersdorf, and H. Ebert, Phys. Rev. B **87**, 014430 (2013).
[26] H. Ebert, S. Mankovsky, K. Chadova, S. Polesya, J. Minár, and D. Ködderitzsch, Phys. Rev. B **91**, 165132 (2015).
[27] A. Brataas, Y. Tserkovnyak, and G. E. W. Bauer, Phys. Rev. Lett. **101**, 037207 (2008).
[28] S. S. Kalarickal, P. Krivosik, M. Wu, C. E. Patton, M. L. Schneider, P. Kabos, T. J. Silva, and J. P. Nibarger, J. Appl. Phys. **99**, 093909 (2006).
[29] Y. Ding, T. J. Klemmer, and T. M. Crawford, J. Appl. Phys. **96**, 2969 (2004).
[30] C. Kittel, J. Phys. et le Rad. **12**, 291 (1951).
[31] J. M. Shaw, H. T. Nembach, T. J. Silva, and C. T. Boone, J. Appl. Phys. **114**, 3906 (2013).
[32] B. Heinrich and J. A. C. Bland, *Ultrathin Magnetic Structures II*, Springer Series in Solid-State Sciences (Springer, Berlin, 1994).
[33] R. McMichael and P. Krivosik, IEEE Trans. Magn. **40**, 2 (2004).
[34] B. Heinrich, J. F. Cochran, and R. Hasegawa, J. Appl. Phys. **57**, 3690 (1985).
[35] R. Arias and D. L. Mills, Phys. Rev. B **60**, 7395 (1999).
[36] D. L. Mills and R. Arias, Physica B **384**, 147 (2006), lAW3M-05 Proceedings of the Seventh Latin American Workshop on Magnetism, Magnetic Materials and their Applications.
[37] R. Yilgin, Y. Sakuraba, M. Oogane, S. Mizukami, Y. Ando, and T. Miyazaki, Jpn. J. Appl. Phys. **46**, L205 (2007).
[38] G. Ortiz, A. García-García, N. Biziere, F. Boust, J. F. Bobo, and E. Snoek, J. Appl. Phys. **113**, 043921 (2013).
[39] A. Sakuma, J. Phys. D: Appl. Phys. **48**, 164011 (2015).
[40] P. He, X. Ma, J. W. Zhang, H. B. Zhao, G. Lüpke, Z. Shi, and S. M. Zhou, Phys. Rev. Lett. **110**, 077203 (2013).
[41] J. I. Langford and A. J. C. Wilson, J. Appl. Cryst. **11**, 102 (1978).
[42] T. Graf, C. Felser, and S. S. P. Parkin, Prog. Solid State Ch. **39**, 1 (2011).
[43] N. Tal, D. Mogilyanski, A. Kovacs, H. Naganuma, S. Tsunegi, M. Oogane, Y. Ando, and A. Kohn, J. Appl. Phys. **114**, 163904 (2013).
[44] S. Rodan, A. Alfonsov, M. Belesi, F. Ferraro, and J. T. Kohlhepp, Appl. Phys. Lett. **102**, 242404 (2013).
[45] J. Lindner, K. Lenz, E. Kosubek, K. Baberschke, D. Spoddig, R. Meckenstock, J. Pelzl, Z. Frait, and D. L. Mills, Phys. Rev. B **68**, 060102 (2003).
[46] C. Liu, C. K. A. Mewes, M. Chshiev, T. Mewes, and W. H. Butler, Appl. Phys. Lett. **95**, 022509 (2009).
[47] R. Yilgin, M. Oogane, Y. Ando, and T. Miyazaki, J. Magn. Magn. Mater. **310**, 2322 (2007).
[48] T. Kubota, S. Tsunegi, M. Oogane, S. Mizukami, T. Miyazaki, H. Naganuma, and Y. Ando, Appl. Phys. Lett. **94**, 122504 (2009).
[49] M. C. Hickey and J. S. Moodera, Phys. Rev. Lett. **102**, 137601 (2009).
[50] Z. Celinski and B. Heinrich, J. Appl. Phys. **70**, 5935 (1991).
[51] I. Neudecker, G. Woltersdorf, B. Heinrich, T. Okuno, G. Gubbiotti, and C. Back, J. Magn. Magn. Mater. **307**, 148 (2006).
[52] A. Ruiz-Calaforra, T. Brcher, V. Lauer, P. Pirro, B. Heinz, M. Geilen, A. V. Chumak, A. Conca, B. Leven, and B. Hillebrands, J. Appl. Phys. **117**, 163901 (2015).
[53] M. A. Khasawneh, C. Klose, W. P. Pratt, and N. O. Birge, Phys. Rev. B **84**, 014425 (2011).